Contents lists available at ScienceDirect

Arabian Journal of Chemistry

journal homepage: www.ksu.edu.sa

Original article

Improving ruthenium nanoparticle physicochemical properties and chemotherapeutic efficacy by dual-encapsulating with new amphiphilic chitosan and imidazolium ionic liquid

W.N. El-Sayed [a,b], J. Alkabli [a,*], Reda F.M. Elshaarawy [c,d,*], Yasser A. Hassan [e,f,g]

[a] Department of Chemistry, College of Sciences and Arts – Alkamil, University of Jeddah, Jeddah 23218, Saudi Arabia
[b] Department of Chemistry, Faculty of Science, Suez University, Suez, Egypt
[c] Department of Chemistry, Faculty of Science, Suez University, 43533 Suez, Egypt
[d] Institut für Anorganische Chemie und Strukturchemie, Heinrich-Heine Universität Düsseldorf, Düsseldorf, Germany
[e] Department of Pharmaceutics and Pharmaceutical Technology, College of Pharmacy, Al-Kitab University, Kirkuk, Iraq
[f] Department of Pharmaceutics, Faculty of Pharmacy, Delta University for Science and Technology, Gamasa, Egypt
[g] Department of Pharmaceutics and Pharmaceutical Technology, College of Pharmacy, Al-Nukhba University College, Baghdad, Iraq

ARTICLE INFO

Keywords:
Chitosan and imidazolium drevatives
Ru-nanobicomposites
Cytotoxicity
Bax/Bcl2 ratio

ABSTRACT

This study introduces new amphiphilic low-molecular-weight chitosan (ALMC) and imidazolium ionic liquid (IIL) as encapsulating agents for in-situ ruthenium nanoparticles (RuNPs) synthesis, resulting in Ru-nanobicomposites (RNBCs: Ru/IIL, RNBC1; Ru-IIL/ALMC, RNBC2) with mean diameters of (2.16–5.19 nm). RNBCs display remarkable collodial stability with high ζ-potential values ((+39.95)–(+48.07) mV) and uniform size distribution with low polydispersity index values (0.23–0.21). *In vitro* experiments revealed that RNBCs had potent anti-cancer properties, with IC_{50} values indicating that they were more toxic to HepG2 cells (IC_{50} = 2.16 ± 0.17–9.12 ± 0.71 μg/ml) than CaCo-2 cells (IC_{50} = 0.61 ± 0.25–11.05 ± 0.48 μg/ml). Specifically, IIL and ALMC's dual-encapsulated RuNPs (RNBC2) could be a potential anticancer drug. RNBC2 increased intrinsic apoptotic markers P53 and Bax gene expression and inhibited Topo II, damaging liver cancer cells. These findings show that RuNPs' encapsulating materials affect their interactions with cancer cells and enhance their anticancer capabilities.

1. Introduction

Human hepatoma, also known as hepatocellular carcinoma (HCC), and colon carcinoma (CRC) are two prevalent types of cancer that pose significant health risks to individuals worldwide. These malignancies are characterized by their aggressive nature and potential to metastasize, leading to poor prognoses if not detected and treated early (Yapasert et al., 2020). Treating human hepatoma and colon carcinoma poses significant challenges due to the development of resistance mechanisms and the occurrence of side effects. Resistance to chemotherapy is a major obstacle in the management of these malignancies. Cancer cells acquire resistance through various mechanisms, including altered drug metabolism, increased drug efflux, altered drug targets, and activation of prosurvival signaling pathways. These resistance mechanisms can render standard chemotherapeutic agents ineffective, leading to treatment failure. Additionally, side effects associated with chemotherapy can be debilitating for patients. The toxicities of chemotherapy drugs can affect various organ systems, such as the gastrointestinal tract, bone marrow, and nervous system. These side effects can significantly impact the patient's quality of life and limit the effectiveness of treatment (Anwanwan et al., 2020, Cardenas and Abrishami, 2023). Therefore, the current approaches and future directions in chemotherapeutic treatments for human hepatoma and colon carcinoma involve the use of combination therapies, nanomedicines, and personalized medicine, which hold great promise in overcoming drug resistance and improving treatment outcomes (Qin et al., 2023).

In recent years, nanomedicine has emerged as a promising field for cancer treatment, with nanomaterials such as noble metal nanoparticles (NMNPs) showing great potential for delivering therapeutic agents to tumor sites (Wicki et al., 2015). However, there are still several challenges that need to be overcome for the successful implementation of NMNPs-based cancer nanomedicine. One of the major challenges is the

* Corresponding authors at: Department of Chemistry, Faculty of Science, Suez University, 43533 Suez, Egypt (Reda F.M. Elshaarawy).
E-mail addresses: jabdalsamad@uj.edu.sa (J. Alkabli), reda.elshaarawy@suezuniv.edu.eg (R.F.M. Elshaarawy).

https://doi.org/10.1016/j.arabjc.2024.105655
Received 13 November 2023; Accepted 15 January 2024
Available online 1 February 2024

limited stability and biocompatibility of NMNPs, which can lead to toxicity and unwanted side effects (Giri et al., 2023). Behzad et al. emphasize the importance of developing surface modification techniques to enhance the stability and biocompatibility of NMNPs. By functionalizing the surface of NMNPs with biocompatible polymers or targeting ligands, it is possible to improve their stability in physiological conditions and reduce their toxicity (Behzad et al., 2021). Another challenge is the efficient and targeted delivery of NMNPs to tumor sites. The use of active targeting strategies, such as the conjugation of targeting ligands to NMNPs, enhances their accumulation in tumors. In conclusion, overcoming the challenges associated with NMNPs-based cancer nanomedicine requires the development of surface modification techniques, active targeting strategies, stimuli-responsive drug release systems, and a rigorous evaluation of their safety and efficacy.

Among NMNPs, ruthenium nanoparticles (RuNPs) have gained considerable attention due to their unique physicochemical properties, such as their small size and well-designed morphlogy, and their ability to selectively target tumor cells (Ali et al., 2017, Samir et al., 2023). RuNPs have been shown to exert their anticancer effects through a variety of mechanisms. Firstly, RuNPs can trigger both intrinsic and extrinsic apoptotic pathways, killing cancer cells. This occurs as a result of mitochondrial malfunction and cell death brought on by the generation of reactive oxygen species (ROS). Secondly, RuNPs can inhibit cancer cell proliferation by interfering with cell cycle progression. They can induce cell cycle arrest at specific checkpoints, such as the G1/S or G2/M phases, thereby preventing cancer cells from undergoing uncontrolled division. In addition, RuNPs have the capacity to suppress angiogenesis, which is pivotal for tumor development and spread. They can interfere with signals necessary for angiogenesis, leading to the suppression of new blood vessel formation and subsequent tumor regression (Zhou et al., 2016, Xia et al., 2022). However, RuNPs are often prone to aggregation, oxidation, and other degradation processes, which can significantly limit their stability and functionality (Gutel et al., 2009). Surface modification techniques offer a promising solution to address these challenges and improve the stability of RuNPs.

One commonly employed surface modification technique, to stabilize RuNPs sterically and electrostatically, is the functionalization of RuNPs with ionic liquids (IILs) (Salas et al., 2011, S Campbell et al., 2013). In recent years, the use of imidazolium ionic liquids (IILs) has gained significant attention in the field of RuNPs stabilization due to their unique properties, such as high thermal and chemical stability, low volatility, and tunable solubility (Salas et al., 2011, S Campbell et al., 2013). Moreover, the use of IILs has been shown to improve the size and morphology of the nanoparticles, as well as their dispersibility in various solvents. The stability of MNPs and IILs is due in part to electrostatic and steric interactions that do not alter the surface properties of the nanoparticles (Verma et al., 2019, Hassanpour et al., 2022). Additionally, because of their remarkable physical features, ILs are also suitable environments for the synthesis and stability of RuNPs (S Campbell et al., 2013).

Notably, chitosan was selected as an ideal stabilizing agent due to its inexpensiveness, renewability, ease of chemical modification, and hosting capabilities for entrapping NMNPs via strong interactions between the polymer's amino groups and the metal surfaces (Shukla et al., 2013). Furthermore, chitosan is widely used in a wide range of biomedical application domains thanks to its low toxicity, tailored biodegradability, and high biocompatibility (Geng et al., 2023). In particular, the low molecular weight chitosan (LMC) has been well documented for its potential biological action in numerous biomedical studies, including those on COVID-19, anti-inflammatory, antioxidant, antibacterial, antitumoral, and antiviral activity (Jaber et al., 2022, Kedir et al., 2022).

These impressive findings motivated us to persist in our quest to develop innovative drugs (Elshaarawy et al., 2017, Elshaarawy et al., 2020, Refaee et al., 2022). In this study, we detail the production of novel ionic liquids (IILs) and amphiphilic low molecular weight chitosan (ALMC) as a combined reducing and stabilizing agent for the creation of Ru-nanobiocomposites (RNBCs). Additionally, the pharmacological properties of the RuNPs-based nanocomposites were evaluated.

2. Materials and instrumentations

All chemicals, solvents, and other compounds used in this investigation, along with detailed information on their characteristics and their origins, are found in the electronic supplementary material (ESM†). Our prior research provided us with the raw materials including glycidyldimethylhexadecyl ammonium chloride (GDMHAC), LMC, and cuminyl chloride (**1**). Moreover, the **ESM†** detailed the synthesis and characterization of *N*-benzylidene LMW (BLMC) and imidazolium ionic liquids (IILs, 2a,b). Microanalytical, spectral methods (FTIR, UV–Vis, NMR (^{1}H NMR, ^{13}C NMR, ^{11}B NMR, ^{19}F NMR, and ESI-MS), and physical measurements were used to examine the structural and physical features of new materials. Information on the tools employed in these investigations is found in the **ESM†** as well.

2.1. Preparation of IIL-coated RuNPs (RNBC1)

A full stepwise protocol used for the preparation of the starting materials and intended RNBCs is depicted in Fig. 1. IIL-coated RuNPs were prepared using a protocol modified from Parida et al work (Parida et al., 2022). Briefly, the preparation was carried out by adding 31.11 mg of $RuCl_3$ (0.15 mmol) to 3 mL of IIL (**2b**) and 15 mL of dry THF in a Schlenk flask at room temperature (RT), and then stirring the mixture for 2 h at 750 rpm. The resulting dark yellow solution was then degassed, heated to 80 °C, and stirred for a further 2 h. After cooling the reaction mixture to RT, $NaBH_4$ (30.26 mg, 0.8 mmol) was added while stirring vigorously. The development of RuNPs was indicated by the dark yellow solution's gradual blackening. For the full conversion of ruthenium salt to Ru(0) and the generation of NPs, stirring at room temperature was continued for 24 h. This was verified by UV–Vis spectroscopic analysis. If the broad absorption band in the precursor's spectrum disappears after reduction, it means all the Ru^{+3} ions have been converted to Ru(0) (see Fig. 1).

Afterward, the reaction mixture was centrifuged for 15 min at 8000 rpm and 15 °C to collect the IIL-coated RuNPs (RNBC1). Following this initial centrifugation, RuNPs were re-suspended in a mixture containing 15 mL of acetone and 20 mL of diethyl ether, and the combined mixture was re-centrifuged. One more time, this procedure was repeated. The subsequent step was dissolving the resultant sticky, black substance in 5 mL of methanol and centrifuging it with 25 mL of diethyl ether. At 15 °C, all centrifugations were conducted for 15 min at 8000 rpm. Finally, the resulting glossy black product was vacuum-dried at 35 °C until it reached a constant weight.

2.2. Preparation of ALMC/IIL-coated RuNPs (RNBC2)

50 mg of ALMC (0.1 % W/V) and 500 mg of IIL (**2b**) were dissolved in 50 mL of dry THF and magnetically agitated for 60 min to prepare a homogenous suspension. The solution was then subjected to a 30-minute ultrasonic treatment. After that, 177 mg of $RuCl_3$ is added to the aforementioned solution and stirred at 80 °C for 2 h. Following cooling to RT, 378 mg of $NaBH_4$ was slowly added to the ALMC/IIL/$RuCl_3$ mixture while vigorously stirring. The content was subsequently subjected to a 6-hour ultrasonic treatment to form a homogeneous dispersion. Afterward, the reaction mixture was centrifuged for 15 min at 8000 rpm and 15 °C to collect the Ru-IIL/ALMC (RNBC2). After that, the RNBC2 was washed three times with ultrapure water, ethanol, and finally diethyl ether to remove the unreacted materials. After washing, the obtained product was vacuum-dried at 40 °C until it reached a consistent weight.

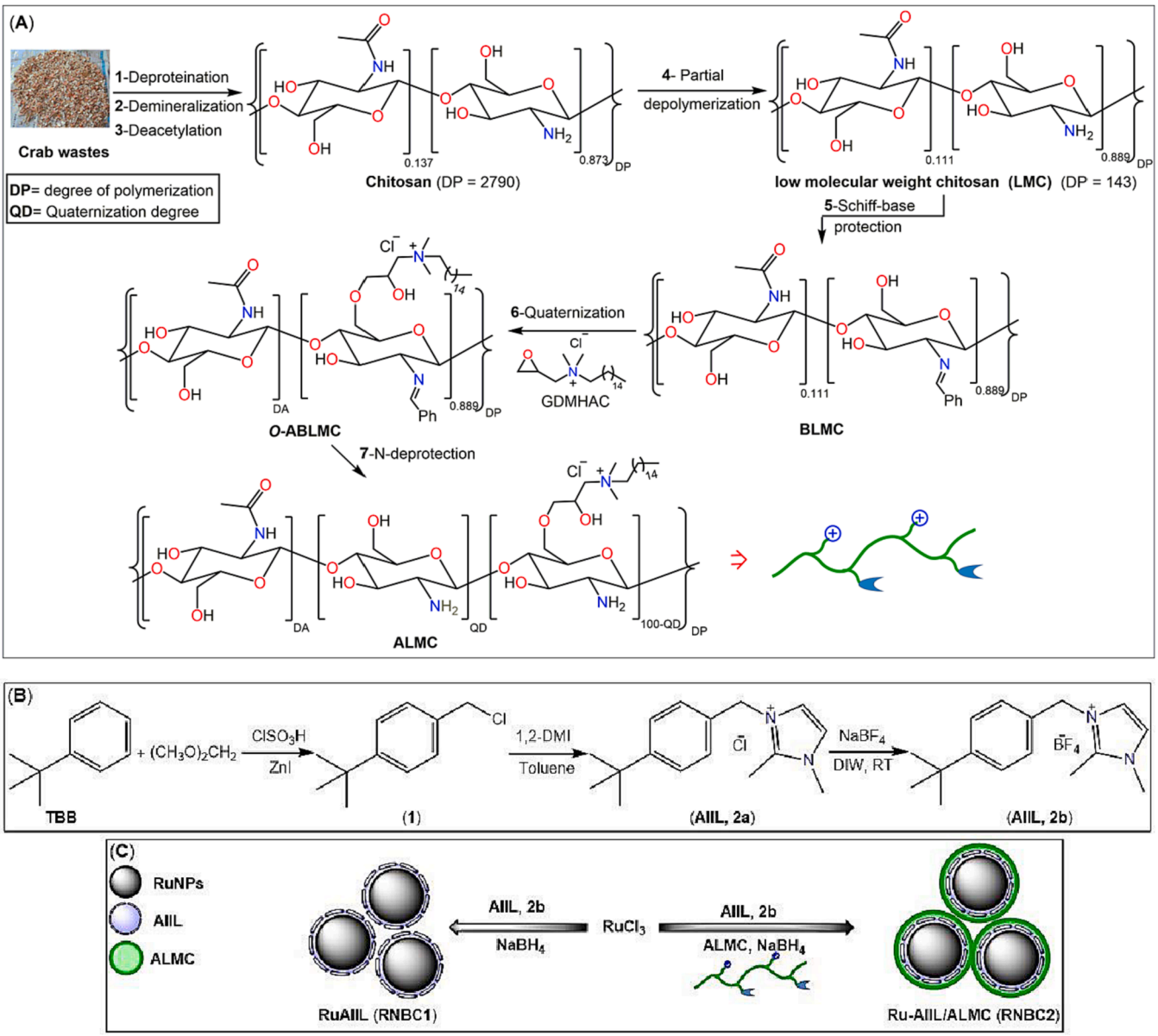

Fig. 1. Step by step synthesis of ALMC (A); IIL (**2b**) (B); and as well thier utlization in the prepration of stablized RuNPs-based NBCs (C).

2.3. Cytotoxicity performance

Two medically significant cancer cells (hepatocellular (HepG2) and colorectal (CaCo-2) carcinomas) as well as normal human liver cells (THLE2) were used to test the novel Ru-nanocomposites' cytotoxic effects. According to our previous studies, we used the MTT assay to perform these analyses, which are described in detail in the **ESM†** (Elshaarawy et al., 2017).

2.4. Gene expression assessment

The expression levels of the P53, BAX, and Bcl2 genes in untreated and NBC2-treated HepG2 cells were compared using the real-time PCR (RT-PCR) method. This was accomplished by culturing HepG2 cells in tissue culture dishes and then treating them with NBC2 at an inhibitory dose (2.16 g/mL) for 24 h. Following the manufacturer's protocol, RNA was initially extracted using a Qiqamp mini kit (Qiagen; USA). The total cellular RNA was then subjected to RT-PCR analysis using one-step QuantiTecht SYBR green (Qiagen; USA) to quantify gene expression of P53, Bax, and Bcl2 before and after NBC2 treatment, according to a previous work (Abdel-Megeed et al., 2022). **Table S1** (**ESM†**) provides the primer sequences and experimental settings used in this analysis. The comparative CT ($2^{-\Delta\Delta CT}$) method was applied to determine the relative expression for each gene (Abdel-Megeed et al., 2022).

2.5. Topoisomerase inhibitory effect

The most potent anticancer agent (RNBC2) was tested for its capacity to inhibit human DNA topoisomerase II (Topo II) using an enzyme-linked immunosorbent assay (ELISA) kit, following the kit's instructions. All of the samples and reagents were set up according to the work processes (Topcu, 2001, Asghar et al., 2023). The protocol used to perform these analyses was described in detail in the **ESM†**.

2.6. Statistical methods

The results of this study were graphically presented, statistically analyzed, and mathematically treated using the programs OriginPro 9.1.32 and SPSS v17. A result was considered to be statistically significant if its P value was < 0.05.

3. Results and discussion

3.1. Synthesis

Intially, a three-step protocol is established to synthesize the desired imidazolium ionic liquids (IILs, **2a,b**) from *tert*-butylbenzene (TBT) (see Fig. 1). To begin, a mixture of dimethoxymethane, chlorosulfonic acid, and zinc iodide was used to chloromethylate TBT, producing 4-(*tert*-butyl)benzyl chloride (TBBC, **1**). Then, in an inert atmosphere, 3-(4'*tert*-butyl benzyl)-1,2-dimethyl imidazolium chloride (**2a**) was prepared by quaternizing 1,2-dimethylimidazole with the TBBC under refluxing conditions. Submitting **2a** to anion metathesis with BF_4^- at under ambient conditions yielded the corresponding imidazolium tetrafluoroborate ionic liquid (**2b**). On the other hand, the amphiphilic low molecular weight chitosan (ALMC) was prepared by *O*-quaternization of LMC with glycidyldimethylhexadecyl ammonium chloride (GDMHAC) through three consecutive reactions: NH_2-protection by Schiff-base condensation, *O*-quaternization, and NH_2-deprotection by acidic hydrolysis. Eventually, the single-layered IIL-encapsulated RuNPs (R**NBC1**) and dual-layered IIL/ALMC-encapsulated RuNPs (R**NBC2**) were prepared by the thermal reduction of its chloride precursor ($RuCl_3$) using $NaBH_4$ as a reducing agent and mediated with IIL/THF or IIL/ALMC/THF, as a green solvent and stabilizing agent, in an inert environment.

3.2. Physicochemical characterization

3.2.1. Physical characterization

An excellent yield of IIL (**2b,** 81.9 %) was realized, and the resulting yellow oil had a density of 1.621 g/cm^3 and an intrinsic viscosity [η] of 439.25 *cP*. In addition, thermogravimetric analysis (TGA) (**Fig. S1, ESM†**) demonstrates that **2b** has high thermal stability (decomposition temperature 399 °C). An important factor in nanoparticle formation, molecular transport, and stability is IL-viscosity. Extremely viscous media, such as ILs, dramatically inhibit nanoparticle diffusion, increasing nanoparticle stability and extending lifetime by a factor of ten-thousand times compared to that in conventional low-viscosity solvents (Kraynov, 2011). IIL **2b**'s high viscosity also offers the another advantage *via* lowering the chance of agglomeration of RuNPs by preventing their thermal mobility.

On the other hand, the η values for the aqueous solutions of LMC and ALMC in NaCl (0.1 M) were measured and used to calculate their average molecular weight (M_{av}) using MHS equation (**Eq. (1)**) (El-Sayed et al., 2021a,b):

$$[\eta] = K\,(M_{av})^{\alpha} \quad (1)$$

The values of M_{av} were calculated as 24.51 KDa for LMC, while 39.37 KDa ALMC, which correspond to polymerization degree (DP) of ~ 143 and ~ 141, respectively.

The ζ-potential was used to test the physical stability of novel Ru nanocomposites (RNBC1 and RNBC2) in water. **Table S2** (**ESM†**) shows that, consistent with their cationic character, both the RuNPs-based nanocomposites and their stabilizers (IIL and ALMC) exhibited highly positive ζ-potential values. Interstingly, the ζ-potential of both nanocomposites exceeds the characterised stability limit for nanoformulations (30 mV) (Hassan et al., 2022). Furthermore, RNBC2 had a higher ζ-potential than RNBC1, indicating that RNBC2 has greater physical stability.

3.2.2. Structural characterization

At first, we used the outcomes of the titrimetric and elemental analyses (EA) to determine the deacetylation degree (DD%) of LMC and the quaternization degree (QD) of ALMC as reported in our previous work (El-Sayed et al., 2021a,b). The findings of these calculations were represented in **Table S2** (**ESM†**). Noteworthy, ALMC's N/C ratio is lower than that of LMC's, indicating that the quaternization process was successful. Moreover, the EA results for ALMC are inconsistent with a full quaternization of the amino group for LMC with the GDMHAC fragment, implying a partial quaternization.

Inductively coupled plasma-atomic emission spectroscopy (ICP-AES) analysis was used to measure the amounts of Ru present in RNBC1 and RNBC2. The Ru contents in the RNBC1 and RNBC2 were 165300 ppm (16.53 w%) and 199200 ppm (19.92 %), respectively. The higher content of RuNPs in the hybrid IIL/ALMC -based nanobiocomposite (RNBC2) compared to the only IIL-based nanobiocomposite (RNBC1) can be attributed to the combined effects of the stabilizing properties of both components, the increased surface area and binding sites for nanoparticle deposition provided by chitosan, and the synergistic interactions between the IIL and ALMC.

ESI-MS (electrospray ionization mass spectrometry) is an essential technique for studying the structural characteristics of ionic liquids. In this context, the ESI-MS of IIL (**2b**) was measured, and the spectrum was given in the **ESM†** (**Fig. S2**). **2b** exhibits a major peak at *m/z* 243.2 a.m.u., corresponding to the molar mass of a monovalent cation formed owing to the departure of the BF_4 anion $[M - BF_4^-]^+$. In addition, several fragmentation peaks were observed at *m/z* 187.1, 172.3, and 157.1 a.m.u. assignable to the consecutive departure of isobutene $[M - BF_4^- - C_4H_8]^+$ and methyl radicals $[M - BF_4^- - CH_3]^+$ & $[M - BF_4^- - 2\,(CH_3)]^+$ from the native IIL, respectively.

The FTIR spectrum of IIL (**2b**) (**Fig. S3, ESM†**) shows absorption bands at 3157, 2960, 1600, 1196, 874, 702, and 581 cm^{-1}, which are related to the vibrational modes of stretching associated with benzylimidazolium cation (alkyl C—H, C═N, and benzyl groups) (Ibrahim et al., 2008, Sidek et al., 2017, El-Sayed et al., 2021a,b). Additionally, the characteristic (BF_4) vibration band can be seen at 1065 cm^{-1} (Elshaarawy and Janiak, 2014). On the other hand, typical vibration bands for LMC (O—H/N—H, 3398 cm^{-1}; bending N—H, 1649 cm^{-1}; amide C═O, 1589 cm^{-1}; and glycoside (C—O—C) group 837 cm^{-1}) and GDMHAC fragment (methyl groups, 2958, 2881 cm^{-1}; R_4N^+, 1511 and 669 cm^{-1}) may be seen in the spectru of ALMC (**Fig. S4, ESM†**). However, with significant alterations due to the grafting reaction, is indicative of its successful (El-Sayed et al., 2021a,b). As for the ruthenium architectures (RNBC1 and RNBC2), it is clear that RuNPs have been immobilized in the IIL (**2b**) matrix for RNBC1 and the IIL/ALMC matrix for RNBC2 due to the profound impacts of nanoruthenium on the distinctive peaks of FTIR spectra for both matrices. Specifically, the OH, NH_2, and C═O peaks at 3389, 1600, and 1593 cm^{-1} were shifted (see Fig. 2**A**) due to their interactions with the RuNPs.

The absence of the distinctive peak associated with the ruthenium precursor ($RuCl_3$) in the spectra of the nanocomposites (as shown in Fig. 2**B**) suggests that the reduction of ruthenium ions (Ru^{3+}) has been effectively achieved through the use of NaBH4, facilitated either by IIL or an IIL-ALMC combination. As an ionic liquid, IIL has a high solubility for both polar and non-polar compounds. This property allows for better dispersion and interaction between the Ru(III) ion and the reducing agent, enhancing the efficiency of the reduction reaction. Moreover, the low viscosity of IIL facilitates mass transfer and diffusion of reactants, ensuring efficient contact between the Ru(III) ion and the reducing agent (Schmolke et al., 2019). On the other hand, the IIL-ALMC combination may facilitates the reduction of Ru(III) ions to Ru(0) in the presence of $NaBH_4$ in several ways. Firstly, the interactions between IIL and ALMC may lead to the formation of a stable microenvironment. This microenvironment provides a confined space where the reduction reaction can take place efficiently. Secondly, the ALMC can coordinate with the Ru(III) ions, forming complexes that enhance the reactivity of the Ru(III) ions towards the reducing agent, $NaBH_4$. This coordination promotes the transfer of electrons from $NaBH_4$ to the Ru(III) ions, facilitating the reduction process. Additionally, the presence of ALMC helps in stabilizing the reduced RuNPs formed during the reduction reaction, preventing their agglomeration and ensuring their uniform dispersion (Zein et al., 2024). According to these results, Ru^{3+} has been converted entirely to Ru(0).

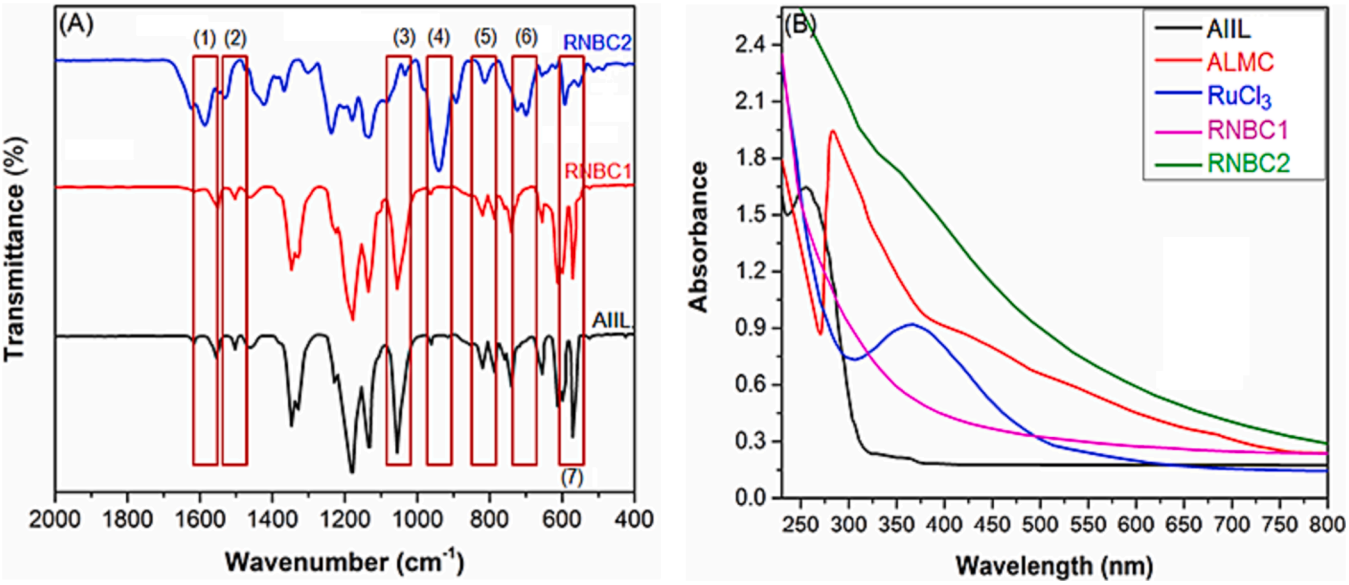

Fig. 2. (**A**) FTIR spectra of IILs (**2b**), IIL-coated RuNPs (RNBC1), and IIL/ALMC-coated RuNPs (RNBC2) showing the major destinctive absorbtion bands: (1), C═N; (2), R_4N^+; (3), BF_4; (4), glycoside group; (5), imidazolium cation; (6), benzyl group. (**B**) UV–Vis spectra of IILs (**2b**), ALMC, $RuCl_3$, RNBC1, and RNBC2.

The ^{1}H NMR spectrum of IIL (Fig. S5, **ESM**†) reveals two distinct proton peak configurations. Two doublets and a multiplet in the 7.74–7.62 ppm range, which can be attributed to the the protons in imidazolium and phenyl resonances, were seen in the first down-field set. In contrast, multiple singlet peaks can be observed in the first high-field set (5.41–1.41 ppm), ascribed to the resonances of the benzylic, *tert*-butyl, and methyl protons. Meanwhile, the ^{13}C NMR spectrum of IIL (Fig. S6, **ESM**†) shows two sets of carbon signals in the low-field (160.28–121.08 ppm) and high-field (50.31–9.87 ppm) regions, corresponding to the resonances of the carbon skeleton for the benzylimidazolium cation and alkyl side chains, respectively. In addition, a two singlets in the ^{11}B NMR (−148.28 ppm) and ^{19}F NMR (−1.29 ppm) spectra of IIL (Fig. S7–8, **ESM**†) further verify the presence of counter tetrafluoroborate anion in this ionic liquid. On the other hand, the ^{1}H NMR spectrum of ALMC exhibits remarkable changes as compared to that of LMC (Fig. S9, **ESM**†). Specifically, the ALMC spectra almost completely lacked the NH_2 signal distinctive of LMC (5.18 ppm), indicating a great quaternization degree. In addition, a new singlet appeared at 3.22 ppm, and multiplet peaks appeared between 3.50 and 0.88 ppm, possibly representing methyl and hexadecyl proton resonances in the GDMHAC segment.

3.3. Morphological characterization

The TEM nanograph of IIL-coated RuNPs (RNBC1) illustrated in Fig. 3**A** shows the formation of a thin film of IIL around nanoparticles, which acts as a monolayer protective shell formed of IIL encasuplating the RuNPs. This shell effectively mitigates nanoparticle aggregation, enabling the RuNPs to maintain a homogeneous dispersion within the mixture. Moreover, the RuNPs exhibited a primarily spherical morphology, characterized by a mean particle diameter (MPD) of 2.16 nm, as depicted in Fig. 3**C**. This MPD was calculated by measuring the diameters of 75 individual nanoparticles from its TEM picture using ImageJ software, and finally calculating the average diameter. Additionally, the RuNPs displayed a low degree of polydispersity (PDI = 0.23), suggesting a uniform size distribution of the nanoparticles. Regarding the double-layered coated ruthenium nanoparticles (RNBC2), the presence of a stiff protective shell effectively inhibits the agglomeration of the ruthenium nanoparticles (as shown in Fig. 3**B**), resulting in their uniform dispersion within a homogeneous mixture. Moreover, the RuNPs exhibited a primarily spherical morphology, characterized by a mean particle diameter (MPD) of 5.19 nm as depicted in Fig. 3**D**. Additionally, the RuNPs displayed a low PDI value of 0.21, suggesting a uniform size distribution of the RuNPs. Overall, the TEM image provides

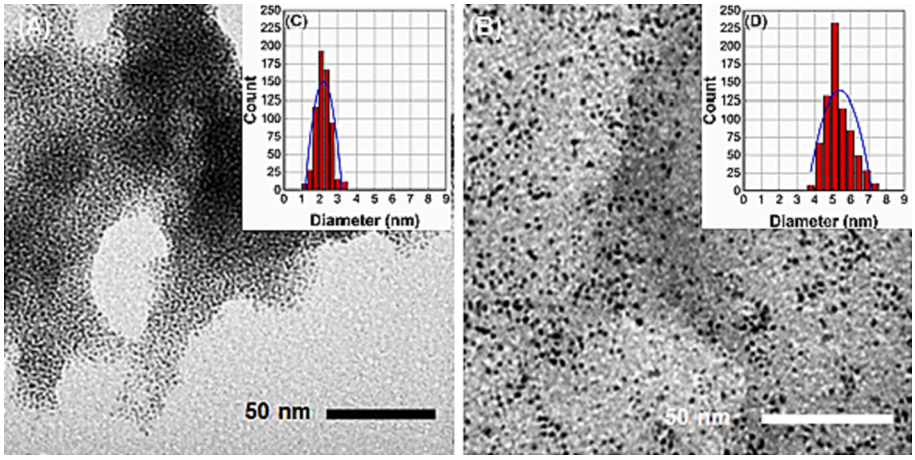

Fig. 3. TEM images of RuNPs-based nanocomposites: (A) RNBC1 and (B) RNBC2. PSD histograms of: RuNPs (C) RNBC1 and (D) RNBC2.

visual evidence of the effectiveness of the protective shell in maintaining the dispersion of ruthenium nanoparticles, offering promising opportunities for their utilization in various scientific and technological domains.

3.4. Cytotoxicity studies

The cytotoxic activity of RNBCs was tested *in vitro* using the MTT assay on two different medically relevant cancer cell lines (HepG2 and CaCo-2). One of the most powerful anticancer drugs, staurosporine (STP), was utilized as a standard in this investigation (Chae et al., 2000). The CaCo-2 and HepG2 cell proliferation as a function of successive concentrations of these nanocomposites is shown in Fig. 4**A,B**. The results demonstrated a statistically significant ($P < 0.05$) reduction in the viability of CaCo-2 and HepG2 cells following treatment with RNBCs. Additionally, the RNBC dose and cell line type affected anticancer effectiveness differently. Meanwhile, HepG2 cells respond to treatments substantially better than CaCo-2 cells do. Furthermore, the RNBC2 nanocomposite outperformed the RNBC1. Overall, the higher cytotoxicity of RNBCs could be attributed to their ultra-small size. The findings of this study align with previous research indicating that the size of nanoparticles (NPs) plays a crucial role in determining their cytotoxicity. The smaller the NPs, the more significant the negative impact on the viability of cancer cells (Lewinski et al., 2008). The small size and special hydrophilic coating of RuNPs allow them to penetrate the cell membrane more efficiently than larger ones, which can result in more significant damage to the cellular structure. Futhermore, the higher surface area to volume ratio of smaller RuNPs, which may increase the amount of reactive oxygen species (ROS) produced upon contact with cells. ROS are known to cause cellular damage and lead to oxidative stress, which can ultimately result in cell death (Lewinski et al., 2008).

According to the data presented in Table 1, the IC_{50} values for RNBC2 were determined to be 2.16 ± 0.17 μg/ml against HepG2 cells and 4.59 ± 0.25 μg/ml against CaCo-2 cells. These findings indicate that RNBC2 exhibits the highest efficacy as an anticancer medication against both cancer cells. Comparatively, the IC_{50} values for RNBC1 were 9.12 ± 0.71 μg/ml against HepG2 and 11.05 ± 0.48 μg/ml against CaCo-2 cells, indicating that it was less cytotoxic toward these cancer cell lines. Most crucially, when tested for cytotoxicity against normal cells, the new RNBC2 had a high IC_{50} value of 25.81 ± 1.45 μg/ml, indicating that they had little impact on healthy cells (THLE2). Thus, compared to normal THLE2 cells, cancer cells were more susceptible to RNBC2's toxicity, as measured by a greater selectivity index (SI) values ($SI_{HepG2/\ CaCo\text{-}2}$ = 11.94/ 5.61. Furthermore, the RNBC2 could be a more secure and effective anticancer candidate than the commercial anticancer compound (STS) ($SI_{HepG2/\ CaCo\text{-}2}$ = 1.65/ 3.95). Therefore, Further studies on the effects of the ruthenium nanocomposite on the expression levels of enzymes P53, Bax, and Bcl2, as well as topoisomerase II activity, are crucial for gaining a comprehensive understanding of the mechanism underlying its anticancer effect. By investigating these specific aspects, we can unravel the intricate interactions between the nanocomposite and key cellular pathways involved in cancer development and progression. Such investigations will not only enhance our knowledge of the therapeutic potential of this nanocomposite but also pave the way for the development of more targeted and effective treatments for cancer.

Table 1
IC_{50} values (μg/ml) of the encapsulated RuNPs (RNBC1 and RNBC2) toward the eximaned cells.

Sample	Cell line	RNBC1	RNBC2	STP
IC_{50} ± SEM (μg/ml)	HepG2	9.12 ± 0.71	2.16 ± 0.17	10.94 ± 0.53
	CaCo-2	11.05 ± 0.48	4.61 ± 0.25	4.14 ± 0.31
	THLE2	37.65 ± 1.76	25.81 ± 1.45	16.33 ± 0.92
SI[a] (HepG2/ CaCo-2)		4.13/ 3.41	11.94/ 5.61	1.65/ 3.95

[a] SI was calculated utilizing the formula (**Eq. 2**) (Alfaifi et al., 2022): $SI = \frac{IC_{50}\ \text{of sample against cancer cells}}{IC_{50}\ \text{of sample against normal cells}}$ (**Eq. 2**).

Interestingly, the anticancer activity of the new Ru-nanobiocomposite (RNBC2) against HepG2 and CaCo-2 is significantly higher than the previously reported RuNPs and ruthenium-complexes (see **Table S3**, **ESM**†). This could be ascribed to the RuNPs possess inherent anticancer properties coupled with the ALMC/IIL vehicles provide a stable and targeted delivery system. This combination allows for the efficient uptake of RNBC2 by cancer cells, leading to enhanced therapeutic effects. The results demonstrated a remarkable improvement in anticancer activity compared to previously studied RuNPs and ruthenium-complexes. This advancement holds great promise for the development of more effective and targeted cancer therapies, potentially offering new treatment options for patients. Further research and clinical trials are needed to fully explore the potential of RNBC2 and its implications in cancer treatment.

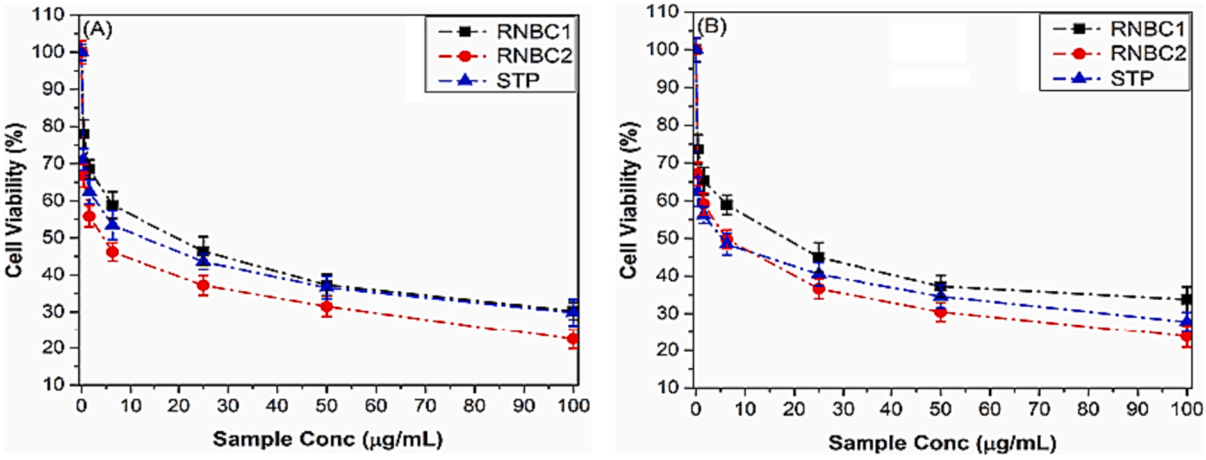

Fig. 4. Comparison of the cytotoxic effects of a clinical anticancer drug (STP) and two new Ru-nanocomposites against (A) HepG2 and (B) CaCo-2 cells as a function of dose.

3.5. Topoisomerase II inhibitory activity

Topoisomerase is an enzyme that helps to regulate DNA topology in cells, and its activity can affect gene expression, cellular metabolism and other important cellular functions. Therefore, it is crucial to research how topoisomerase activity is affected by RNBC2, how this biochemical reaction occurs, and how this effect may be applied for potential medicinal and therapeutic purposes. To that objective, the inhibition of topoisomerase II (Topo II) by RNBC2 was studied. When compared with control HepG2 (Topo II = 489.2 ± 23.8 ng/mL), Topo II activity is significantly decreased ($p < 0.01$) when HepG2 cells treated with RNBC2, with a resulting value of 181.4 ± 6.11 ng/mL (see Fig. 5**A**). Interestingly, RNBC2 was a more potent inhibitor of the Topo II enzyme than the chemotherapeutic inhibitor Staurosporine (STS) which can lower the enzyme to 208.9 ± 4.39 ng/mL (57.2 % reduction compared to control HepG2), while RNBC2 was able to decrease the Topo II enzyme to 181.4 ± 6.11 ng/mL, a reduction of 62.9 % compared to HepG2 control (see Fig. 5**A**). This great inhibitory effect was thought to be due to the direct interaction between the RuNPs and the topoisomerase enzyme, inhibiting cellular activities related to DNA replication and transcription. Furthermore, RuNPs have also been found to induce oxidative stress in cells, leading to damage to proteins, lipids, and DNA (Cai et al., 2017). These results demonstrate that RNBC2 have a significant impact on topoisomerase activity, suggesting that RNBC2 may be used as a potential chemotherapeutic tool to target topoisomerase activity. In addition, RNBC2 could potentially be used in future treatments to modulate gene expression and other cellular functions.

3.6. Effect of the RNBC2 on P53, Bax and Bcl2 expressions in HepG2 cells

The regulation of apoptosis is a complex process intimately linked to the balance between pro- and anti-apoptotic signaling pathways. P53, Bax, and Bcl2 are major players in the regulation of this process. P53 is a tumor suppressor gene that can induce and initiate apoptosis by upregulating Bax and downregulating Bcl2. Bax is a proapoptotic protein that can induce cytochrome *c* release from the mitochondria and activate the caspase cascade. Bcl2 is an anti-apoptotic protein that can inhibit cytochrome *c* release and prevent activation of the caspase cascade. Together, P53, Bax, and Bcl2 are integral components of the apoptotic cascade and are essential for the proper regulation of cell death and survival (Brambilla et al., 1996, Basu, 2022). Therefore, investigations have been done into how RNBC2 affects the expressions of P53, Bax, and Bcl2 enzymes (See Fig. 5). After HepG2 cells were exposed to the IC_{50} dosage of RNBC2 for 24 h, the levels of P53, Bax, and Bcl2 were assessed by ELISA. Fig. 5**A,B** demonstrates that, in comparison to untreated HepG2 cells, Bax and P53 levels were substantially increased in RNBC2-treated HepG2 cells (five- and six-times, respectively). Contrary, the decrease in Bcl2 (fourfold) was much smaller in RNBC2-treated HepG2 cells compared to uninfected cells. As can be seen from these data, apoptosis in HepG2 cells is induced by RNBC2 in a p53-dependent fashion. Upon being exposed to RNBC2, HepG2 cells trigger the tumor-suppressor gene p53, which in turn may alter the inner mitochondrial membrane's normal function and lead to a change in membrane potential. These results showed that activation of the pro-apoptotic gene (Bax) suppresses the release of the anti-apoptotic protein (Bcl2). Thus, apoptotic pathways are activated, and cell death occurs, due to the balance between pro- and anti-apoptotic proteins. DNA damage, oxidative stress, and mutations are just some of the things that can set cells on the path to apoptosis.

Notably, the results of zeta potential and morphological properties of Ru nanocomposites play a crucial role in supporting the findings of their superior anticancer activity as well as their capacities to up-regulate P53 and Bax, while down-regulating Bcl2. A high zeta potential indicates a strong electrostatic repulsion between particles, preventing their aggregation. This is important because the nanocomposites need to maintain their stability and remain dispersed in order to effectively interact with cancer cells. Furthermore, the morphological properties of nanoparticles, such as their size, shape, and surface characteristics, also contribute to their anticancer activity. RuNPs with a smaller size generally have a higher surface area, which translates to increased interaction with cancer cells. Additionally, nanoparticles with nanosphere shapes can exhibit enhanced cellular uptake and improved targeting of cancer cells. The ability of Ru nanocomposites to up-regulate P53 and Bax, while down-regulating Bcl2, is another crucial aspect supporting their superior anticancer activity. P53 and Bax are tumor suppressor proteins that play important roles in regulating cell cycle arrest and apoptosis, while Bcl2 is an anti-apoptotic protein that inhibits cell death. The up-regulation of P53 and Bax and the down-regulation of Bcl2 can promote apoptosis in cancer cells, leading to their death. The mechanism through which these nanoparticles achieve the up-regulation of P53 and Bax and the down-regulation of Bcl2 is likely multifaceted. The cationic chitosan/imidazolium coating of the RuNPs may facilitate their internalization into cancer cells and enable the release of the encapsulated ruthenium. Once inside the cells, ruthenium can potentially interact with cellular components, such as DNA or proteins, and trigger signaling pathways that lead to the desired changes in gene expression.

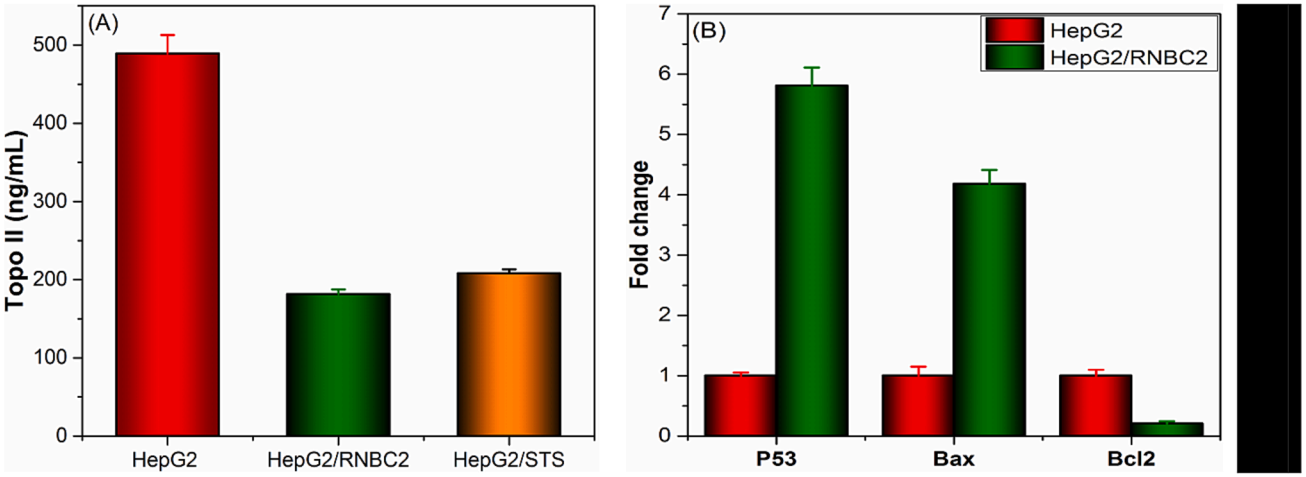

Fig. 5. Topo II activity and changes in p53, Bax, and Bcl-2 gene expression, as measured by polymerase chain reaction (PCR), following 24 h of treatment with RNBC2 (IC_{50} dosage).

4. Conclusion

This study was multi-tasking, initially, new derivatives of imidazolium ionic liquid (IIL) and amphiphilic low-moleular-weight chitosan (ALMC) have been successfully synthesized as well as structurally and mophologically characterized. Therafter, IIL and ALMC were used as encapsulating materials for RuNPs to fabricate Ru-nanobicomposites (RNBCs: Ru/IIL, RNBC1; Ru-IIL/ALMC, RNBC2). The spectral and microscopic techniques validated the success of RNBCs formation. The high ζ-potential values of RNBCs ((+39.95) - (+48.07) mV) indicates a strong electrostatic repulsion between particles, preventing their aggregation, and colloidal stablity. TEM nanographs showed that RuNPs in both RNBCs were mostly nanospheres with low MPD values (2.16–5.19 nm) and polydispersity index (0.23–0.21), suggesting a uniform size distribution. These findings are beneficial for the anticancer potential of the new Ru-nanobicomposites. The *in vitro* tests showed that RNBCs had effective anti-cancer effects, with IC_{50} values that showed that they were more toxic to HepG2 cells than CaCo-2 cells. Specifically, the dual-encapsulated RuNPs by IIL and ALMC (RNBC2) could offer a promising anticancer agent. RNBC2 showed superior Topo II inhibitory activity and was effective in up-regulating P53 and Bax gene expersions, markers of the intrinsic apoptotic pathway, causing damage to liver cancer cells. These findings highlight the importance of the encapsulating materials for RuNPs in their interactions with cancer cells and their potential as effective anticancer agents. Further research in this area can help advance our understanding of the underlying mechanisms and potentially lead to the development of novel and more targeted cancer therapies.

Declaration of competing interest

The authors declare that they have no known competing financial interests or personal relationships that could have appeared to influence the work reported in this paper.

Acknowledgments

This work was funded by the University of Jeddah, Jeddah, Saudi Arabia, under grant No. (UJ-21-DR-129). The authors, therefore, acknowledge with thanks the University of Jeddah technical and financial support.

Appendix A. Supplementary material

Supplementary data to this article can be found online at https://doi.org/10.1016/j.arabjc.2024.105655.

References

Abdel-Megeed, R.M., Ali, S.A., Khalil, W.B., et al., 2022. Mitigation of apoptosis-mediated neurotoxicity induced by silver nanoparticles via rutaceae nutraceuticals: P53 activation and Bax/Bcl-2 regulation. Toxicol. Rep. 9, 2055–2063. https://doi.org/10.1016/j.toxrep.2022.11.009.

Alfaifi, M.Y., Shati, A.A., Elbehairi, S.E.I., et al., 2022. Fine-tuning of the pharmacological potential of novel thiazolium ionic liquids by anion alteration. RSC Adv. 12, 458–469.

Ali, M.Y.S., Anuradha, V., Abishek, R., et al., 2017. In vitro anticancer activity of green synthesis ruthenium nanoparticle from Dictyota dichotoma marine algae. NanoWorld J. 3, 66–71.

Anwanwan, D., Singh, S.K., Singh, S., et al., 2020. Challenges in liver cancer and possible treatment approaches. Biochim. Biophys. Acta (BBA) – Rev. Cancer 1873, 188314. 10.1016/j.bbcan.2019.188314.

Asghar, B.H., Hassan, R.K.A., Barakat, L.A.A., et al., 2023. Cross-linked quaternized chitosan nanoparticles for effective delivery and controllable release of O. europaea phenolic extract targeting cancer therapy. J. Drug Delivery Sci. Technol. 104388 https://doi.org/10.1016/j.jddst.2023.104388.

Basu, A., 2022. The interplay between apoptosis and cellular senescence: Bcl-2 family proteins as targets for cancer therapy. Pharmacol. Ther. 230, 107943.

Behzad, F., Naghib, S.M., Kouhbanani, M.A.J., et al., 2021. An overview of the plant-mediated green synthesis of noble metal nanoparticles for antibacterial applications. J. Ind. Eng. Chem. 94, 92–104. https://doi.org/10.1016/j.jiec.2020.12.005.

Brambilla, E., Negoescu, A., Gazzeri, S., et al., 1996. Apoptosis-related factors p53, Bcl2, and Bax in neuroendocrine lung tumors. Am. J. Pathol. 149, 1941.

Cai, Y., Zhang, J., Chen, N.G., et al., 2017. Recent advances in anticancer activities and drug delivery systems of tannins. Med. Res. Rev. 37, 665–701.

Campbell, S., Hg Prechtl, P.M., Santini, C.C., et al., 2013. Ruthenium nanoparticles in ionic liquids–a saga. Curr. Org. Chem. 17, 414–429.

Cardenas, C.A., Abrishami, S., 2023. Colorectal Carcinoma: Review and Novelties in 2023. Clin. Oncol. Case Rep. 6 (6), 2.

Chae, H.-J., Kang, J.-S., Byun, J.-O., et al., 2000. Molecular mechanism of staurosporine-induced apoptosis in osteoblasts. Pharmacol. Res. 42, 373–381.

El-Sayed, W.N., Alkabli, J., Aloqbi, A., et al., 2021a. Optimization enzymatic degradation of chitosan into amphiphilic chitooligosaccharides for application in mitigating liver steatosis and cholesterol regulation. Eur. Polym. J. 153, 110507 https://doi.org/10.1016/j.eurpolymj.2021.110507.

El-Sayed, W.N., Alkabli, J., Althumayri, K., et al., 2021b. Azomethine-functionalized task-specific ionic liquid for diversion of toxic metal ions in the aqueous environment into pharmacological nominates. J. Mol. Liq. 322, 114525 https://doi.org/10.1016/j.molliq.2020.114525.

Elshaarawy, R.F.M., Eldeen, I.M., Hassan, E.M., 2017. Efficient synthesis and evaluation of bis-pyridinium/bis-quinolinium metallosalophens as antibiotic and antitumor candidates. J. Mol. Struct. 1128, 162–173.

Elshaarawy, R.F.M., El-Azim, H.A., Hegazy, W.H., et al., 2020. Poly(ammonium/pyridinium)-chitosan Schiff base as a smart biosorbent for scavenging of Cu2+ ions from aqueous effluents. Polym. Test. 83, 106244 https://doi.org/10.1016/j.polymertesting.2019.106244.

Elshaarawy, R.F.M., Janiak, C., 2014. Ionic liquid-supported chiral saldach with tunable hydrogen bonding: synthesis, metalation with Fe(III) and in vitro antimicrobial susceptibility. Tetrahedron 70, 8023–8032. https://doi.org/10.1016/j.tet.2014.08.034.

Geng, Y., Xue, H., Zhang, Z., et al., 2023. Recent advances in carboxymethyl chitosan-based materials for biomedical applications. Carbohydr. Polym., 120555

Giri, P.M., Banerjee, A., Layek, B., 2023. A Recent Review on Cancer Nanomedicine. Cancers 15, 2256.

Gutel, T., Santini, C.C., Philippot, K., et al., 2009. Organized 3D-alkyl imidazolium ionic liquids could be used to control the size of in situ generated ruthenium nanoparticles? J. Mater. Chem. 19, 3624–3631.

Hassan, Y.A., Alfaifi, M.Y., Shati, A.A., et al., 2022. Co-delivery of anticancer drugs via poly(ionic crosslinked chitosan-palladium) nanocapsules: Targeting more effective and sustainable cancer therapy. J. Drug Delivery Sci. Technol. 69, 103151 https://doi.org/10.1016/j.jddst.2022.103151.

Hassanpour, M., Shahavi, M.H., Heidari, G., et al., 2022. Ionic liquid-mediated synthesis of metal nanostructures: Potential application in cancer diagnosis and therapy. J. Ionic Liquids. 2, 100033 https://doi.org/10.1016/j.jil.2022.100033.

Ibrahim, H.K., El-Tamany, S.H., El-Shaarawy, R.F., et al., 2008. Synthesis and investigation of mass spectra of some novel benzimidazole derivatives. Macedonian J. Chem. Chem. Eng. 27.

Jaber, N., Al-Remawi, M., Al-Akayleh, F., et al., 2022. A review of the antiviral activity of Chitosan, including patented applications and its potential use against COVID-19. J. Appl. Microbiol. 132, 41–58.

Kedir, W.M., Abdi, G.F., Goro, M.M., et al., 2022. Pharmaceutical and drug delivery applications of chitosan biopolymer and its modified nanocomposite: A review. Heliyon., e10196

Kraynov, A., T. E. J. A. o. i. l. i. s. Müller and technology, 2011. Concepts for the stabilization of metal nanoparticles in ionic liquids. 9, 235-260.

Lewinski, N., Colvin, V., Drezek, R., 2008. Cytotoxicity of Nanoparticles. Small 4, 26–49. https://doi.org/10.1002/smll.200700595.

Parida, D., Bakkali-Hassani, C., Lebraud, E., et al., 2022. Tuning the activity and selectivity of polymerised ionic liquid-stabilised ruthenium nanoparticles through anion exchange reactions. Nanoscale 14, 4635–4643.

Qin, J., Wang, X., Fan, G., et al., 2023. Recent advances in Nanodrug Delivery System for Tumor Combination Treatment based on Photothermal Therapy. Adv. Therap. 6, 2200218.

Refaee, A.A., El-Naggar, M.E., Mostafa, T.B., et al., 2022. Nano-bio finishing of cotton fabric with quaternized chitosan Schiff base-TiO2-ZnO nanocomposites for antimicrobial and UV protection applications. Eur. Polym. J. 166, 111040.

Salas, G., Santini, C.C., Philippot, K., et al., 2011. Influence of amines on the size control of in situ synthesized ruthenium nanoparticles in imidazolium ionic liquids. Dalton Trans. 40, 4660–4668.

Samir, N., Özerkan, D., Danışman-Kalındemirtaş, F., et al., 2023. Synthesis and Anticancerogenic Effect of New Generation Ruthenium-Based Nanoparticle from Homalothecium sericeum with Eco-Friendly Method. J. Pharm. Innov. 1–12.

Schmolke, L., Lerch, S., Bülow, M., et al., 2019. Aggregation control of Ru and Ir nanoparticles by tunable aryl alkyl imidazolium ionic liquids. Nanoscale 11, 4073–4082.

Shukla, S.K., Mishra, A.K., Arotiba, O.A., et al., 2013. Chitosan-based nanomaterials: A state-of-the-art review. Int. J. Biol. Macromol. 59, 46–58.

Sidek, N., Manan, N.S.A., Mohamad, S., 2017. Efficient removal of phenolic compounds from model oil using benzyl Imidazolium-based ionic liquids. J. Mol. Liq. 240, 794–802. https://doi.org/10.1016/j.molliq.2017.05.111.

Topcu, Z., 2001. DNA topoisomerases as targets for anticancer drugs. J. Clin. Pharm. Ther. 26, 405–416. https://doi.org/10.1046/j.1365-2710.2001.00368.x.

Verma, C., Ebenso, E.E., Quraishi, M., 2019. Transition metal nanoparticles in ionic liquids: Synthesis and stabilization. J. Mol. Liq. 276, 826–849.

Wicki, A., Witzigmann, D., Balasubramanian, V., et al., 2015. Nanomedicine in cancer therapy: challenges, opportunities, and clinical applications. J. Control. Release 200, 138–157.

Xia, F., Hu, X., Zhang, B., et al., 2022. Ultrasmall ruthenium nanoparticles with boosted antioxidant activity upregulate regulatory T cells for highly efficient liver injury therapy. Small 18, 2201558.

Yapasert, R., Sripanidkulchai, B., Teerachaisakul, M., et al., 2020. Anticancer effects of a traditional Thai herbal recipe Benja Amarit extracts against human hepatocellular carcinoma and colon cancer cell by targeting apoptosis pathways. J. Ethnopharmacol. 254, 112732 https://doi.org/10.1016/j.jep.2020.112732.

Zein, M.A., Asghar, B.H., Almohyawi, A.M., et al., 2024. Multifunctional nanocomposites integrated green synthesized amphiphilic chitosan/thyme extract/nanosilver for antimicrobial and anti-biofilm applications. React. Funct. Polym. 194, 105791.

Zhou, Y., Yu, Q., Qin, X., et al., 2016. Improving the anticancer efficacy of laminin receptor-specific therapeutic ruthenium nanoparticles (RuBB-loaded EGCG-RuNPs) via ROS-dependent apoptosis in SMMC-7721 cells. ACS Appl. Mater. Interfaces 8, 15000–15012.